Journal of Physics and Chemistry of Solids 145 (2020) 109567

Contents lists available at ScienceDirect

Journal of Physics and Chemistry of Solids

journal homepage: http://www.elsevier.com/locate/jpcs

Fundamental studies of hafnia-hematite nanoparticles

Louise Ferris [a], Mark Allwes [a], Lucian Diamandescu [b], Alice Perrin [c], Michael McHenry [c], Monica Sorescu [a,*]

[a] Duquesne University, Department of Physics, Fisher Hall, Pittsburgh, PA, 15282, USA
[b] National Institute of Materials Physics, Bucharest-Magurele, 77125, Romania
[c] Carnegie Mellon University, Department of Materials Science and Engineering, Roberts Hall, Pittsburgh, PA, 15213, USA

ARTICLE INFO

Keywords:
Oxides
Mössbauer spectroscopy
Magnetic properties

ABSTRACT

$xHfO_2$-(1-x)α-Fe_2O_3 (x = 0.1, 0.3, 0.5 and 0.7) nanoparticles system was obtained using mechanochemical activation by high energy ball milling for time periods ranging from 0 to 12 h. X-ray diffraction patterns revealed the presence of two phases, a hafnium-doped hematite and an iron-doped hafnia, which competed with each other to form a solid solution. The trend observed in the lattice parameters using Rietveld refinement was consistent with differences in ionic radii between Hf and Fe. Crystallite sizes for both hematite and hafnia were analyzed as function of milling time using the Scherrer method and found to decrease down to ~15 nm for all molar concentrations used. Mössbauer spectroscopy revealed the presence of 1–5 sextets corresponding to different numbers of Hf nearest neighbors of Fe in the hematite structure. The different hyperfine magnetic fields could be resolved in the model of local atomic environment. Substitutions of Fe in hafnia gave rise to a nonmagnetic phase represented by a quadrupole split doublet, whose abundance was found to increase with ball milling time. Hysteresis loops recorded at 5 K showed that the Hf-doped system does not saturate in an applied magnetic field of 5 T. The Morin transition was observed during zero-field-cooling-field cooling (ZFC-FC) in an external magnetic field of 200 Oe. Differential scanning calorimetry with thermal gravimetric analysis (DSC-TGA) evidenced an exothermic peak for the starting oxides and an endothermic peak for the solid solution.

1. Introduction

Hafnia-lanthanide oxide system (HfO_2-Ln_2O_3) has been intensively studied, in view of the potential significance of hafnia in nuclear technology, such as control rods, neutron shielding and structural devices [1–13]. This is because hafnium (Hf) and many of the lanthanides have high thermal-neutron-capture cross sections. Moreover, hafnia can be tailored to different degrees of neutron absorption, while maintaining its refractory nature.

However, mixed oxides of hafnia and iron oxides have not been studied to date. In particular, hafnia-hematite system attracts interest due to its prospective nanotechnology applications [14]. In the present study we propose to synthesize hafnia-hematite nanoparticles by mechanochemical activation and further investigate their structural and magnetic properties by X-ray diffraction, Mössbauer spectroscopy, magnetic measurements and thermal analysis.

2. Materials and methods

Nanoparticles of $xHfO_2$-(1-x)α-Fe_2O_3 (x = 0.1, 0.3, 0.5 and 0.7) have been obtained using mechanochemical activation, starting from precursors of hafnia and hematite powders with an average particle size of 50 nm and purity better than 99.9%.

Samples of hafnia and hematite were introduced in a SPEX 8000 mixer mill and ground for time periods ranging from 0 to 12 h. The 8000 M Mixer/Mill is a high-energy ball mill that grinds up to 0.2–10 g of dry, brittle samples. The vial, which contains a sample and one or more balls, is shaken in a complex motion that combines back-and-forth swings with short lateral movements, each end of the vial describing a Fig. 8. The clamp's motion develops strong G-forces in the vial, to pulverize the toughest rocks, slags and ceramics. In our experiments the powder: ball mass ratio was 1:5.

The powder diffraction patterns (XRD) of the hafnia-hematite ball-milled samples were recorded with a PANalytic X'Pert Pro MPO diffractometer with CuK_α radiation (λ = 1.54187 Å). An X'cellerator

* Corresponding author. Duquesne University, Department of Physics, 600 Forbes Avenue, 309 B Fisher Hall, Pittsburgh, PA, 15282, USA.
E-mail address: sorescu@duq.edu (M. Sorescu).

https://doi.org/10.1016/j.jpcs.2020.109567
Received 26 March 2020; Received in revised form 13 May 2020; Accepted 16 May 2020
Available online 20 May 2020
0022-3697/© 2020 Elsevier Ltd. All rights reserved.

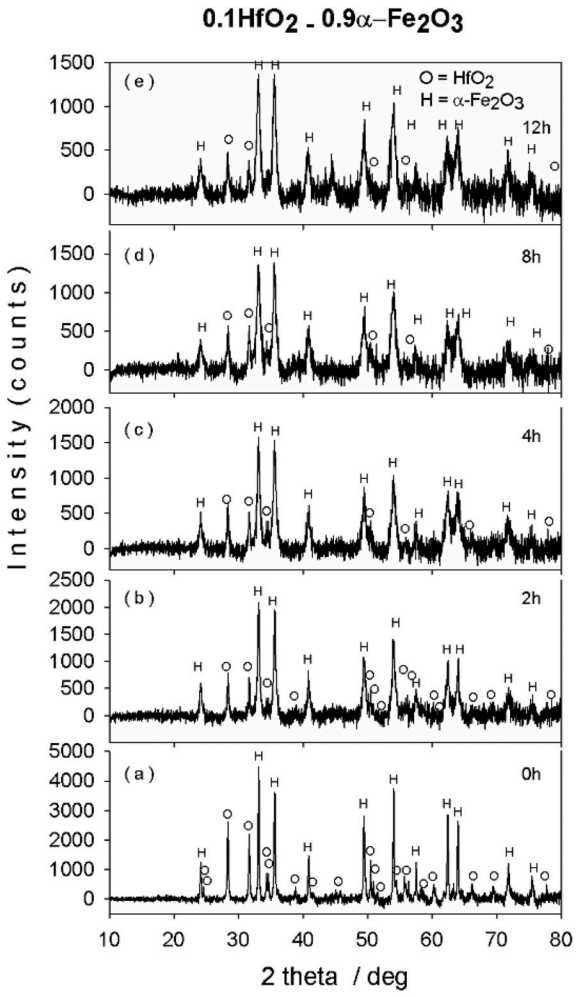

Fig. 1. X-ray diffractograms of ball milled hafnia-hematite (x = 0.1) after periods of (a) 0 h; (b) 2 h; (c) 4 h; (d) 8 h; (e) 12 h.

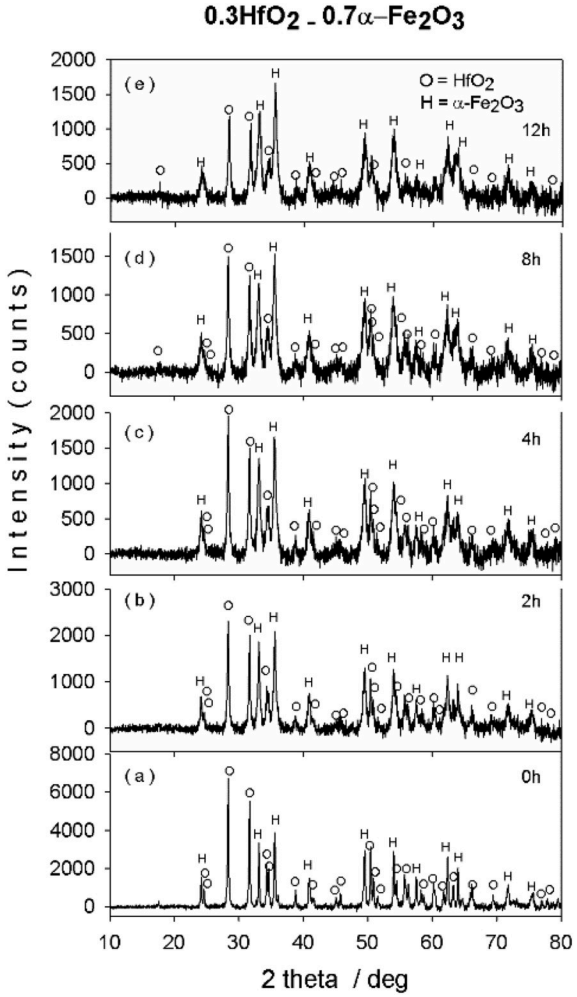

Fig. 2. X-ray diffractograms of ball milled hafnia-hematite (x = 0.3) after periods of (a) 0 h; (b) 2 h; (c) 4 h; (d) 8 h; (e) 12 h.

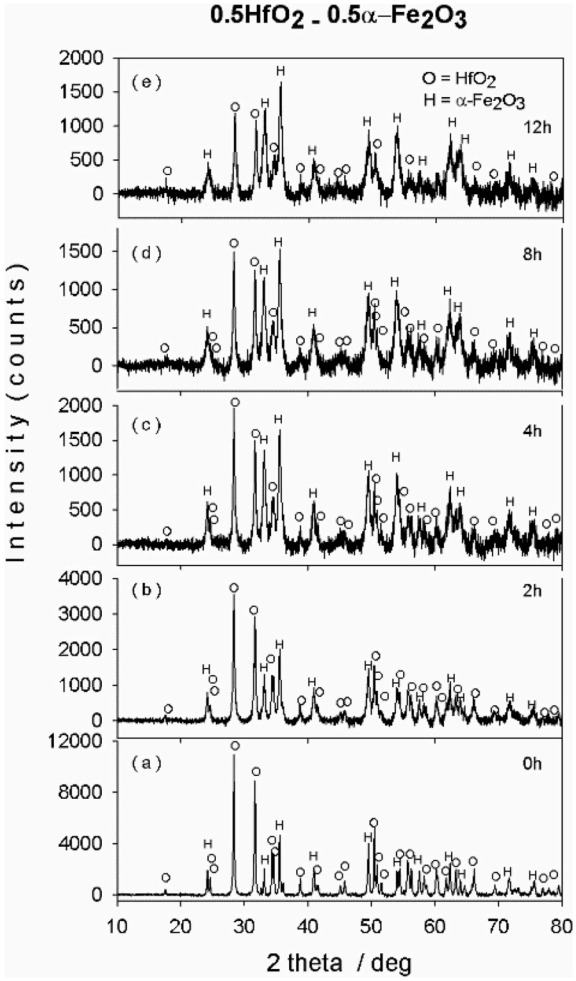

Fig. 3. X-ray diffractograms of ball milled hafnia-hematite (x = 0.5) after periods of (a) 0 h; (b) 2 h; (c) 4 h; (d) 8 h; (e) 12 h.

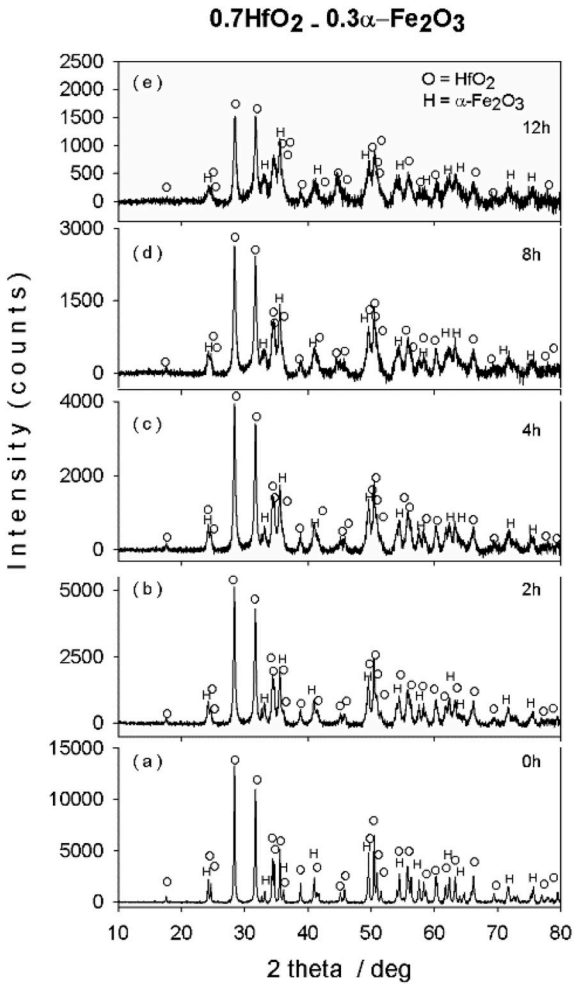

Fig. 4. X-ray diffractograms of ball milled hafnia-hematite (x = 0.7) after periods of (a) 0 h; (b) 2 h; (c) 4 h; (d) 8 h; (e) 12 h.

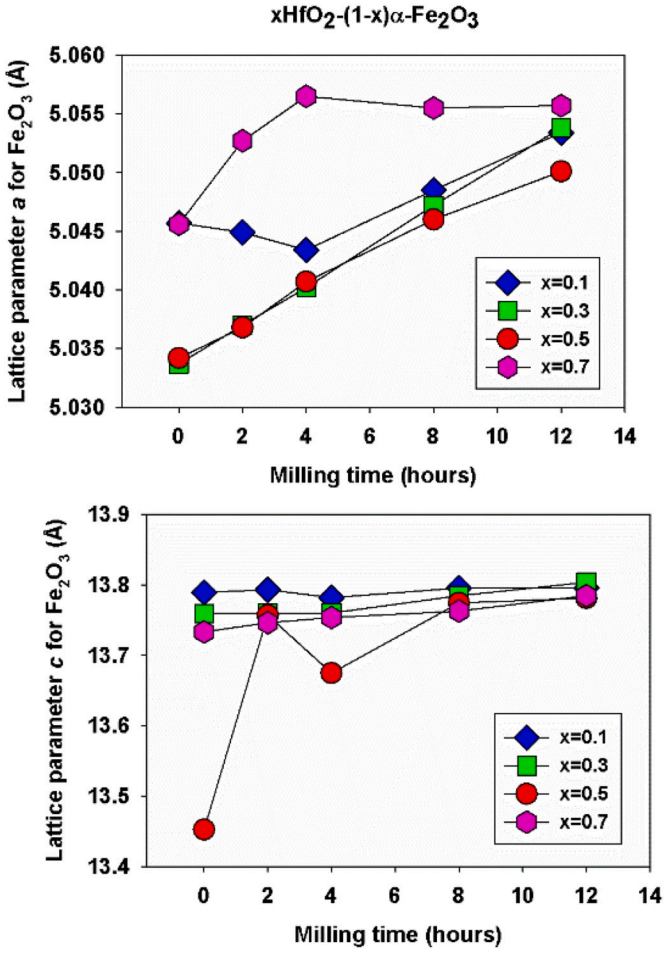

Fig. 5. Lattice parameters *a* and *c* for hematite.

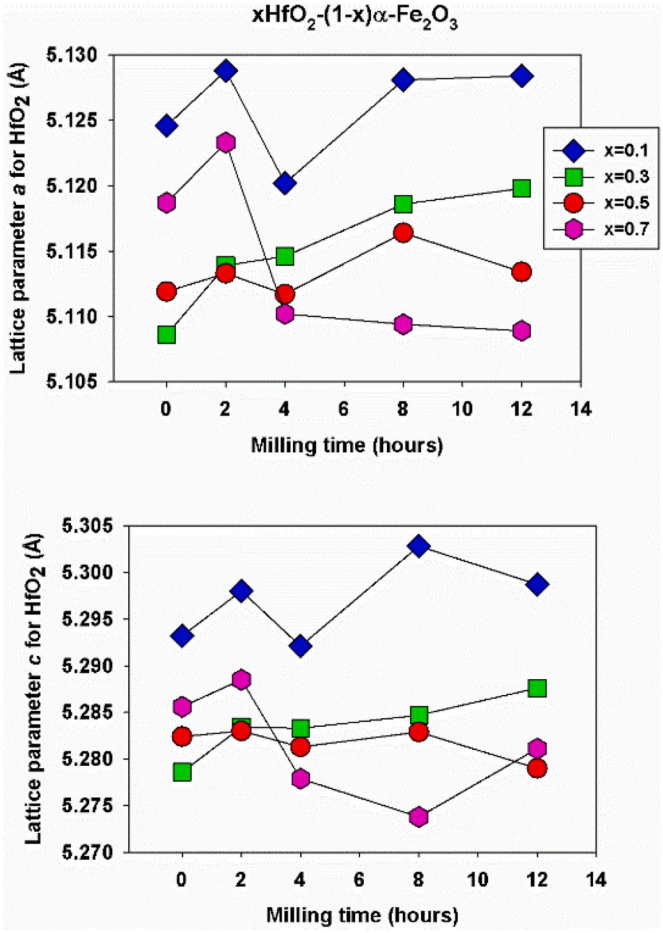

Fig. 6. Lattice parameters *a* and *c* for hafnia.

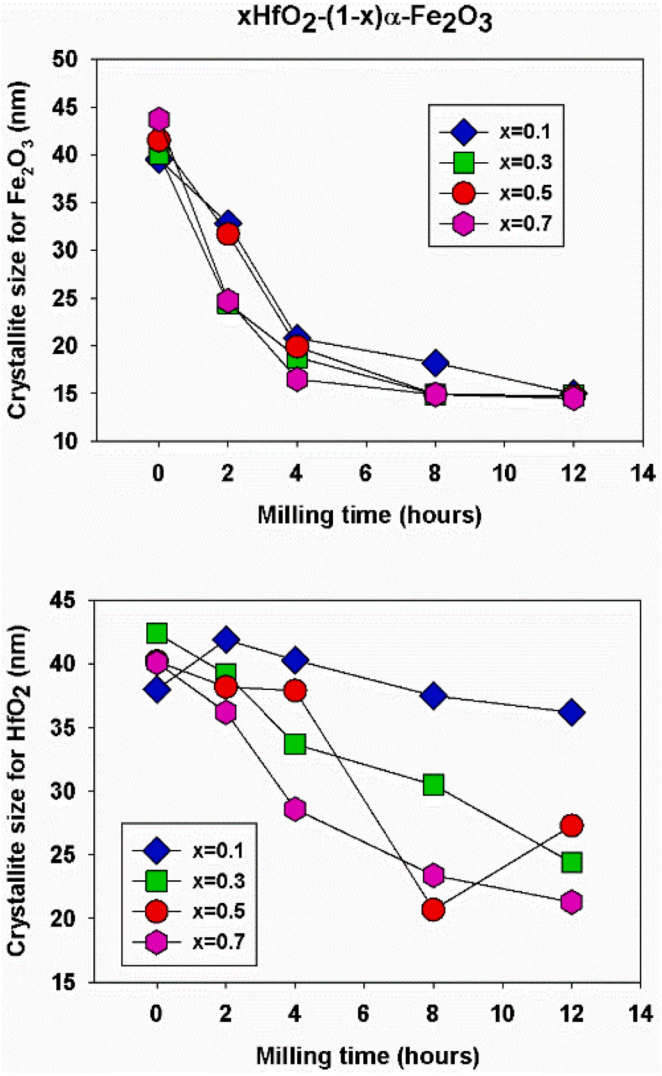

Fig. 7. Crystallite sizes for hematite and hafnia.

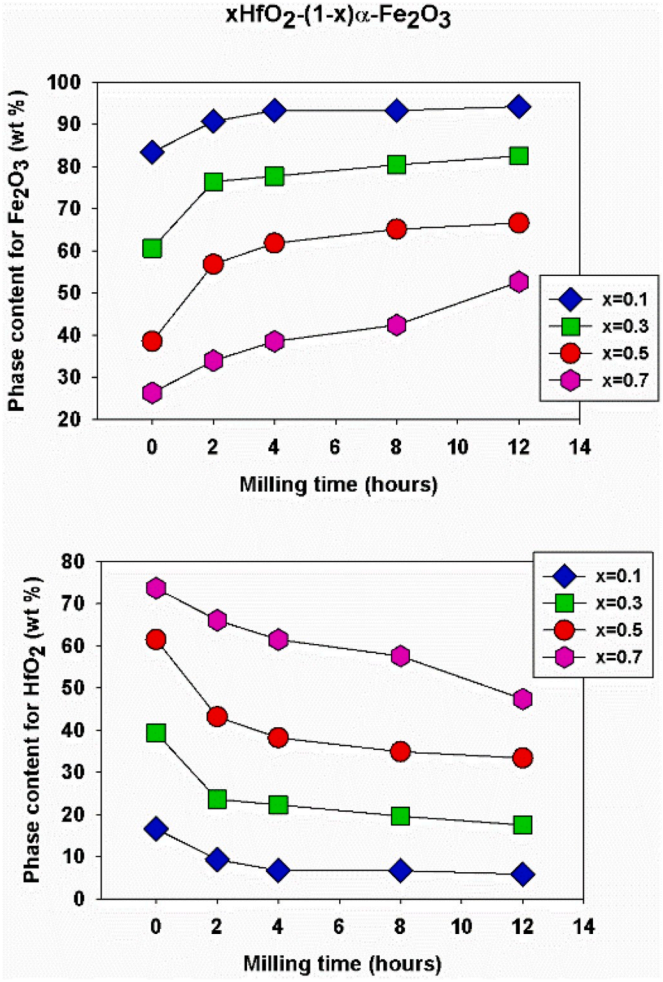

Fig. 8. Phase content for hafnia and hematite.

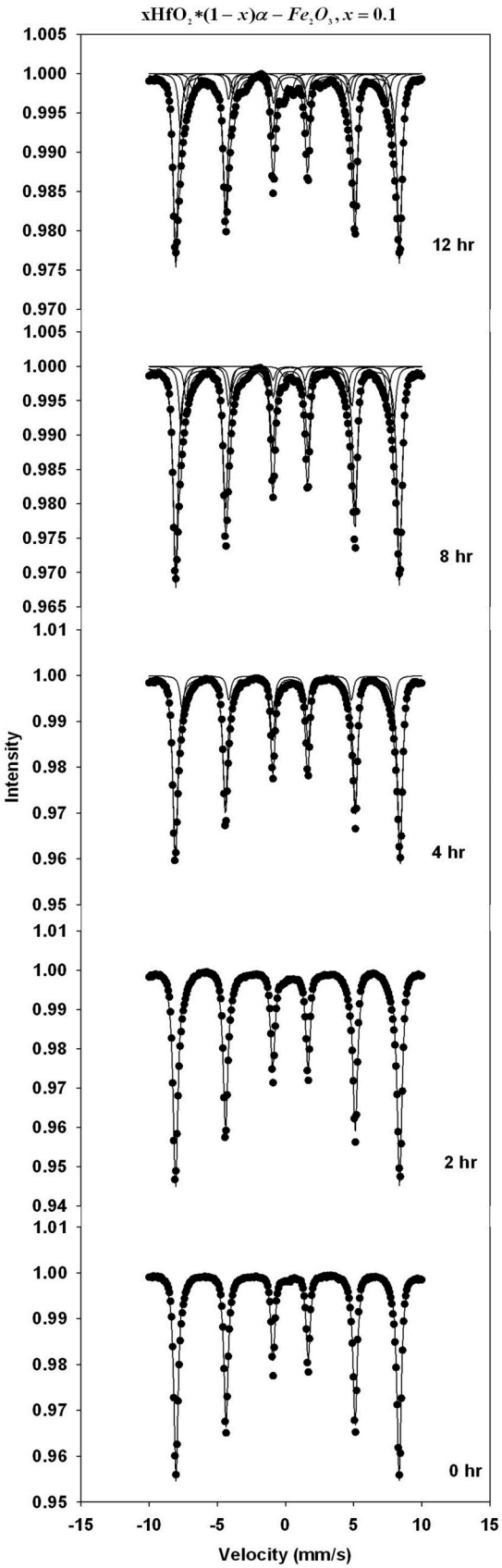

Fig. 9. Mössbauer spectra of ball-milled hafnia and hematite (x = 0.1) for milling times of 0–12 h.

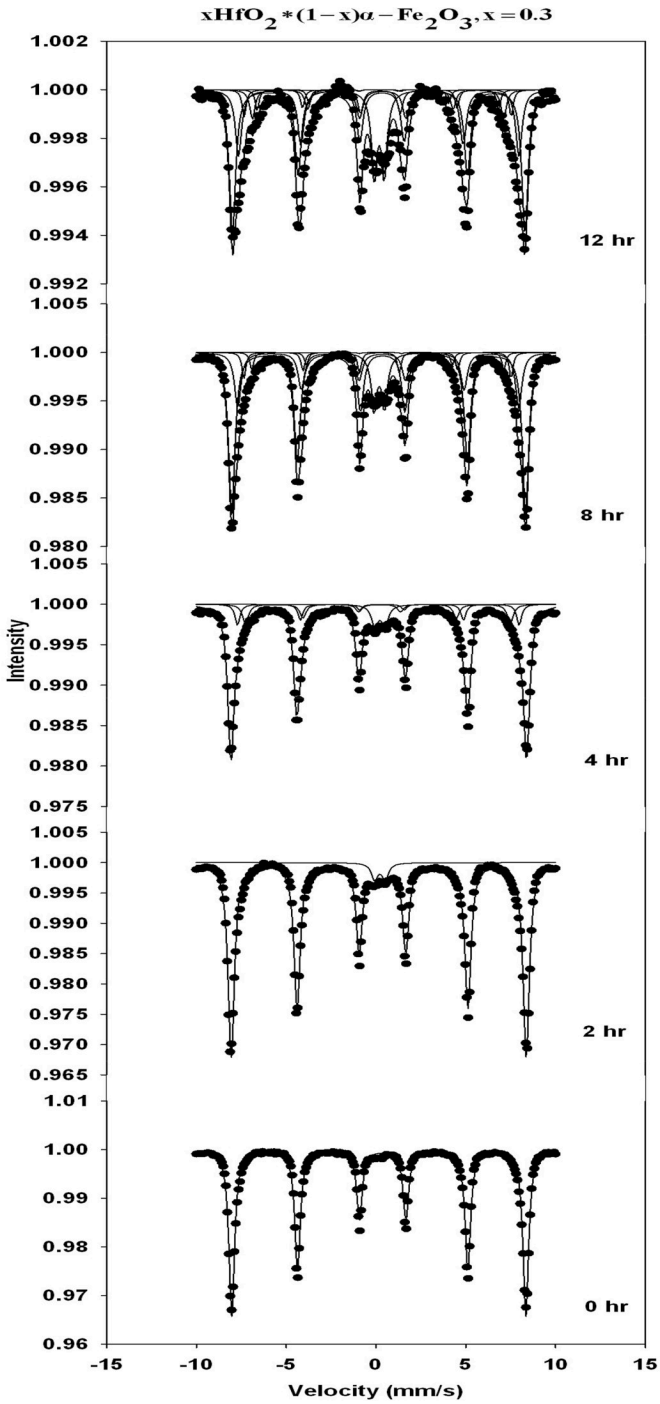

Fig. 10. Mössbauer spectra of ball-milled hafnia and hematite (x = 0.3) for milling times of 0–12 h.

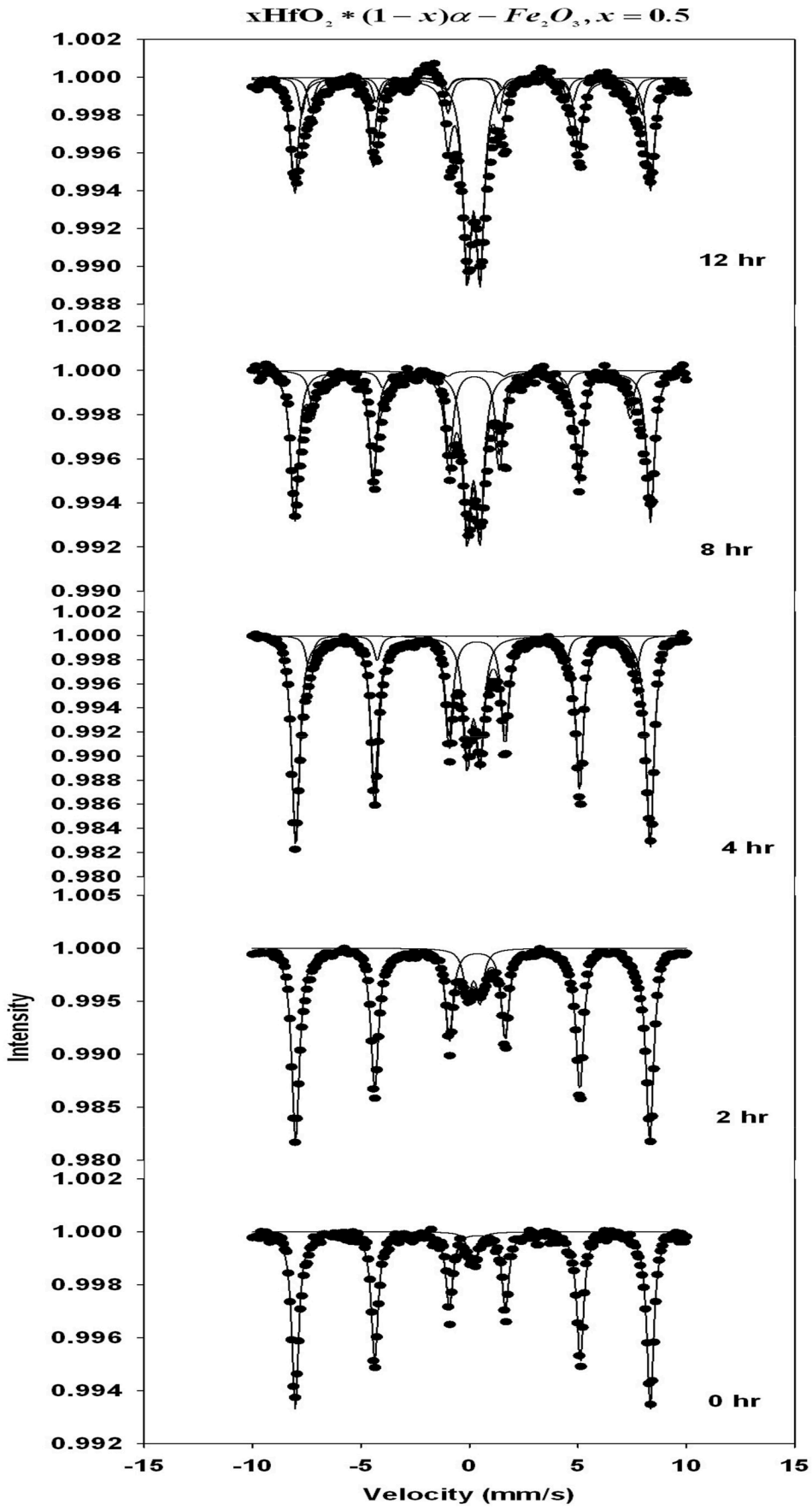

Fig. 11. Mössbauer spectra of ball-milled hafnia and hematite (x = 0.5) for milling times of 0–12 h.

detector was used, with a diffraction angle 2θ = 10-80° and a preselected step size of 0.02°. The average crystallite size was derived using the Scherrer method for all studied molarities. The XRD patterns were analyzed using Rietveld refinement, which yielded the lattice parameters as function of ball milling time.

The room-temperature transmission Mössbauer spectra were recorded using a SeeCo constant accelerator spectrometer equipped with a 25 mCi ^{57}Co gamma ray source. Hysteresis loop measurements were recorded with a Quantum Design SQUID magnetometer in a temperature interval of 5–300 K and an applied magnetic field of 5 T, while the zero-field cooling was performed at 200 Oe.

Simultaneous DSC-TGA experiments were performed using a Netzsch Model STA 449F3 Jupiter instrument with a SiC furnace. Samples weighting 15 ± 1 mg were contained in a manufacturer's alumina crucible with an alumina lid. The atmosphere consisted of flowing protective argon gas at a rate of 50 mL/min. The DSC and TGA curves were obtained by heating samples from room temperature to 800 °C with a ramp rate of 10 °C/min. The Netzsch Proteus Thermal Analysis software was used for DSC and TGA data analysis.

3. Results and discussion

The XRD diffractograms of hafnium dioxide-hematite nanoparticle system, $xHfO_2(1\text{-}x)\alpha\text{-}Fe_2O_3$ are reproduced in Figs. 1–4(a)-(e). They correspond to different ball milling times (BMT = 0–12 h) and different molarities, x = 0.1, 0.3, 0.5 and 0.7. As the ball milling time is increased, the XRD diffractograms exhibit peak broadening, which can be related to a decrease in crystallite sizes for both oxides involved. Moreover, the peak intensities decrease as well, which could be due to consumption of the reacted materials.

Fig. 5 presents the dependence of lattice parameters *a* and *c* for hematite on ball milling time for each value of the molar concentration studied. The lattice parameters were extracted from the XRD patterns using the Rietveld refinement method. It was found that parameter *a* increases with the ball milling time, while parameter *c* kept constant values. This trend in lattice parameters is consistent with Hf substituting Fe in the hematite lattice, which correlates well with the respective values of the ionic radii, 78 p.m. for Hf^{4+} and 63 p.m. for Fe^{3+}. Similar trends in the lattice parameters *a* and *c* were observed for HfO_2 as function of ball milling time for all concentrations studied and plotted in Fig. 6.

Fig. 7 displays the crystallite size for hematite and hafnia as function of ball milling time and all molarities. The crystallite size was obtained from the XRD patterns using the Scherrer method. It was determined that the crystallite sizes for hematite and hafnia decreased as function of milling times down to 15 and 20 nm, respectively. This decrease in grain size, correlated with the increase in lattice distortions and ion substitutions is expected to lead to lattice parameters changes, as observed in Fig. 6.

Fig. 8 indicates that the hafnium-doped hematite phase increases, while the hafnia content is diminished as function of ball milling time for all values of the molarities employed. This is consistent with Hf substituting hematite as function of processing parameters.

Figs. 9–12 display the transmission Mössbauer spectra recorded at 300 K for the hafnia-hematite nanoparticles system, at different molar concentrations and ball milling times. Figs. 13 and 14 show the magnetic hyperfine field (BHF) as function of ball milling time (BMT) for all systems studied, as well as the abundance of the quadrupole split doublet as function of processing parameters. The spectra corresponding to 0 h of milling time were analyzed considering one sextet with BHF of 51.65 T, representing hematite. As the milling time increased, additional sextets became present in the deconvolution of the Mössbauer spectra, with decreasing values of BHF. Indeed, according to the model of local atomic environment, substitution of Fe ions with nonmagnetic Hf ions decreases the BHF at iron sites and causes the appearance of several sextets in the Mössbauer spectra, depending on the number of Hf nearest

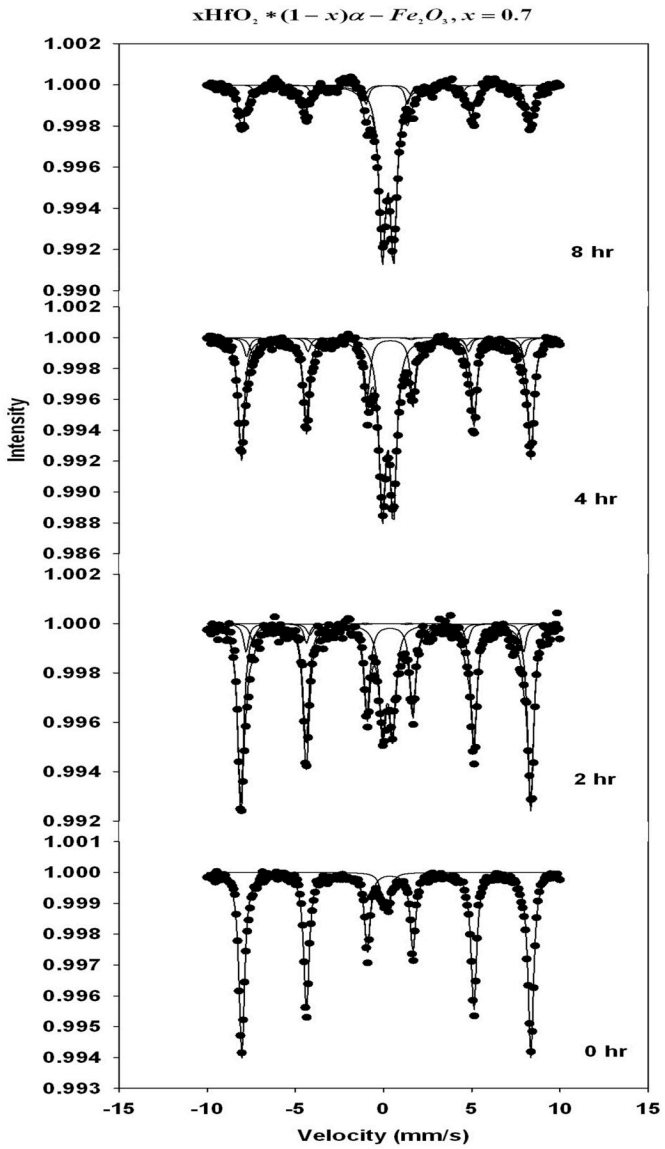

Fig. 12. Mössbauer spectra of ball-milled hafnia and hematite (x = 0.7) for milling times of 0–8 h.

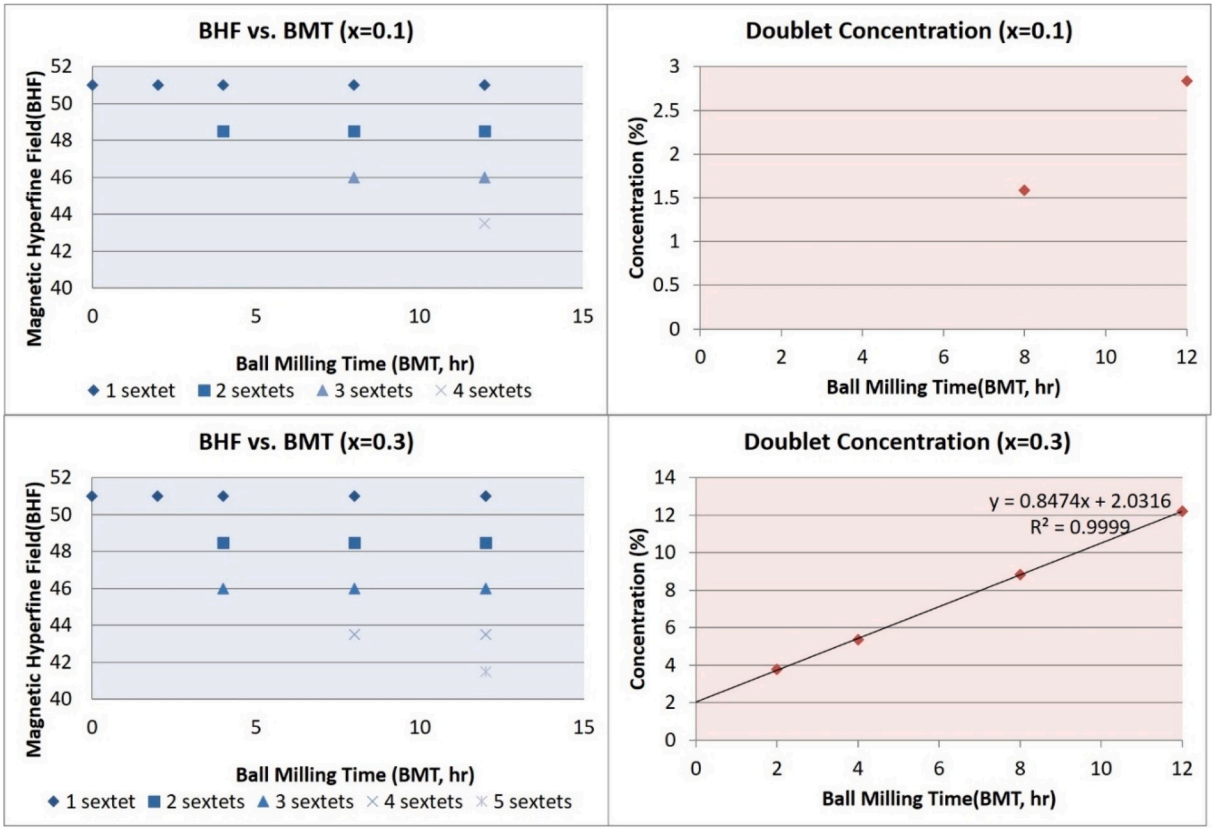

Fig. 13. Hyperfine magnetic field and doublet concentration as function of milling time for x = 0.1 and 0.3.

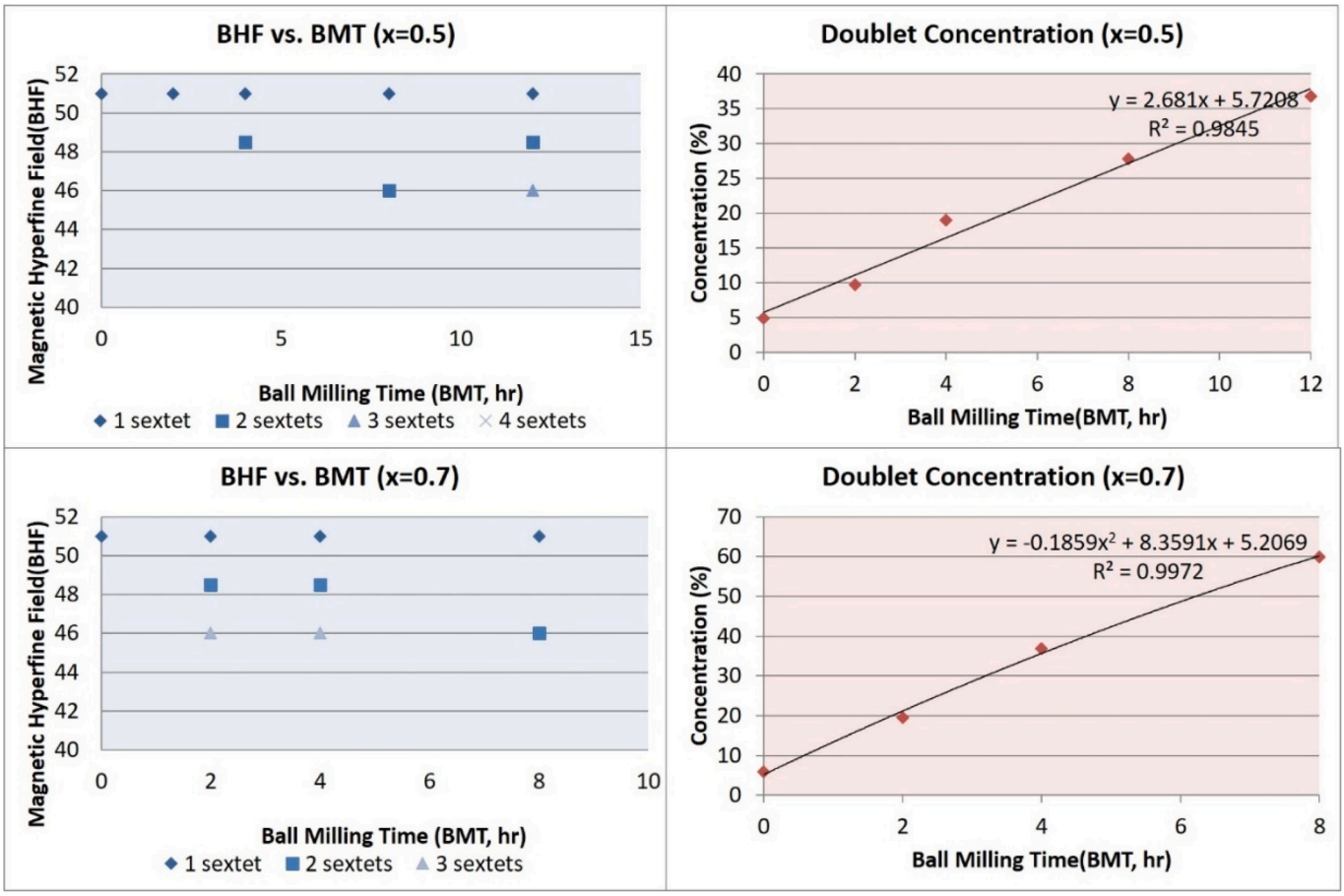

Fig. 14. Hyperfine magnetic field and doublet concentration as function of milling time for x = 0.5 and 0.7.

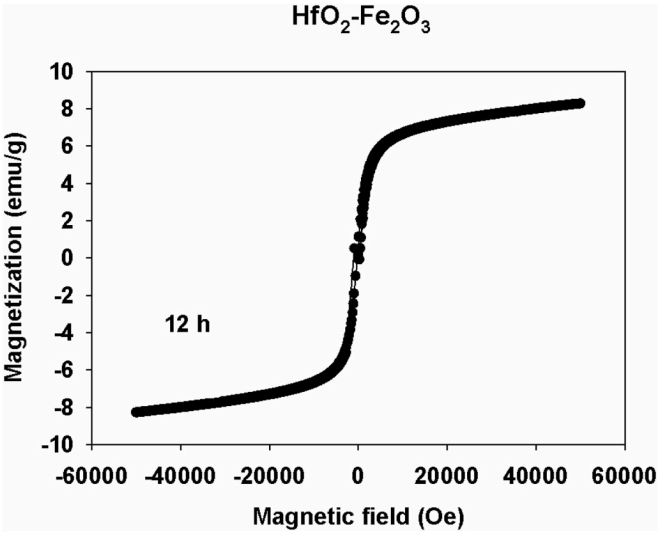

Fig. 15. Hysteresis loop of the equimolar hafnia-hematite system after 12 h of milling, recorded at 5 K and 5 T applied magnetic field.

neighbors. On the other hand, substitutions of Hf ions with Fe ions in the hafnia lattice gives rise to a nonmagnetic phase represented by a quadrupole-split doublet, whose abundance increases as function of milling time, as can be seen in Figs. 13 and 14. The plots are guides to the eye.

Fig. 15 presents the hysteresis loop of hafnia-hematite equimolar mixture, recorded at 5 K with an applied magnetic field of 5 T, after a 12-h ball milling period. It can be seen that saturation is not reached even in the magnetic field of 5 T. The remanent magnetization is close to 0.23 emu/g and the coercive field is 0.025 Oe, which is practically vanishing coercivity.

Fig. 16 shows the zero-field-cooling-field-cooling (ZFC-FC) curves recorded for the hafnia-hematite system (x = 0.5) with an applied magnetic field of 200 Oe in the temperature interval 5–300 K, after having been exposed to milling for times of 0, 4 and 12 h. As the milling time increases, the average crystallite size decreases and the hematite Morin temperature takes lower values, which are spread over a temperature interval. For these reasons the transformation resembles an incline instead of a step.

Differential scanning calorimetry with thermal gravimetric analysis (DSC-TGA) is presented in Figs. 17 and 18 for the equimolar mixture of hafnia and hematite after 0 and respectively, 12 h of milling. The figures evidence an exothermic peak for the starting oxides and an endothermic peak for the solid solution. This endothermic peak stayed the same for the milled composition for all milling times. The occurrence of the peaks in DSC is accompanied by slopes in the TGA curves. This thermal analysis nicely complements the XRD and Mössbauer results.

4. Conclusions

We have successfully synthesized hafnia-hematite nanoparticles system using mechanochemical activation by high energy ball milling at four different molar concentrations and different processing parameters. Its structural, magnetic and thermal properties were analyzed using XRD, Mössbauer spectroscopy, magnetic measurements and DSC-TGA. They were used to obtain a wealth of fundamental information on lattice parameters, crystallite size, phase composition, hyperfine parameters, magnetic properties and thermal behavior. Hafnia is now ready for neutron absorption applications.

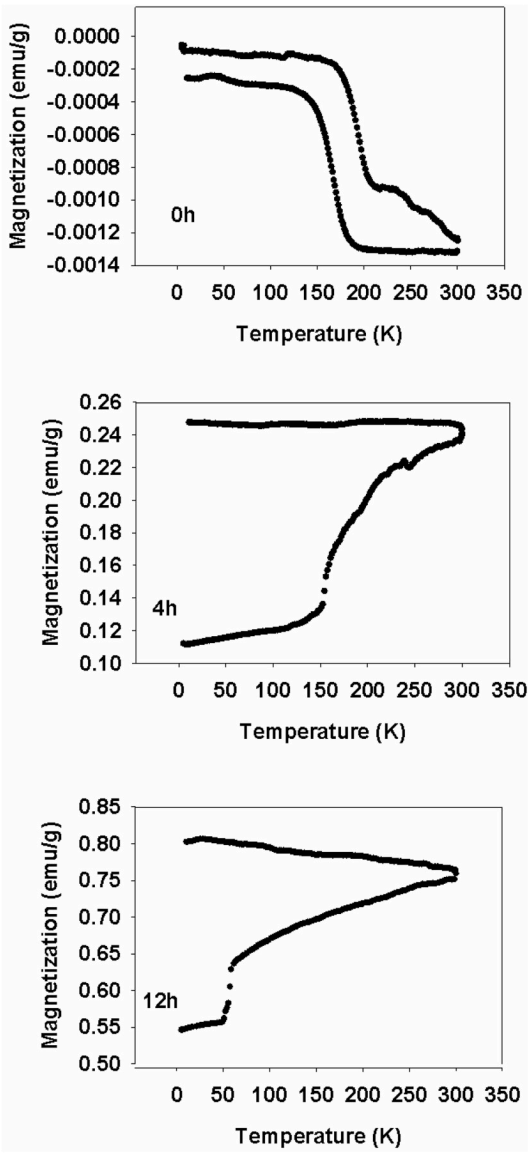

Fig. 16. ZFC-FC at 200 Oe and 5–300 K for equimolar hafnia-hematite samples after milling at 0, 4 and 12 h.

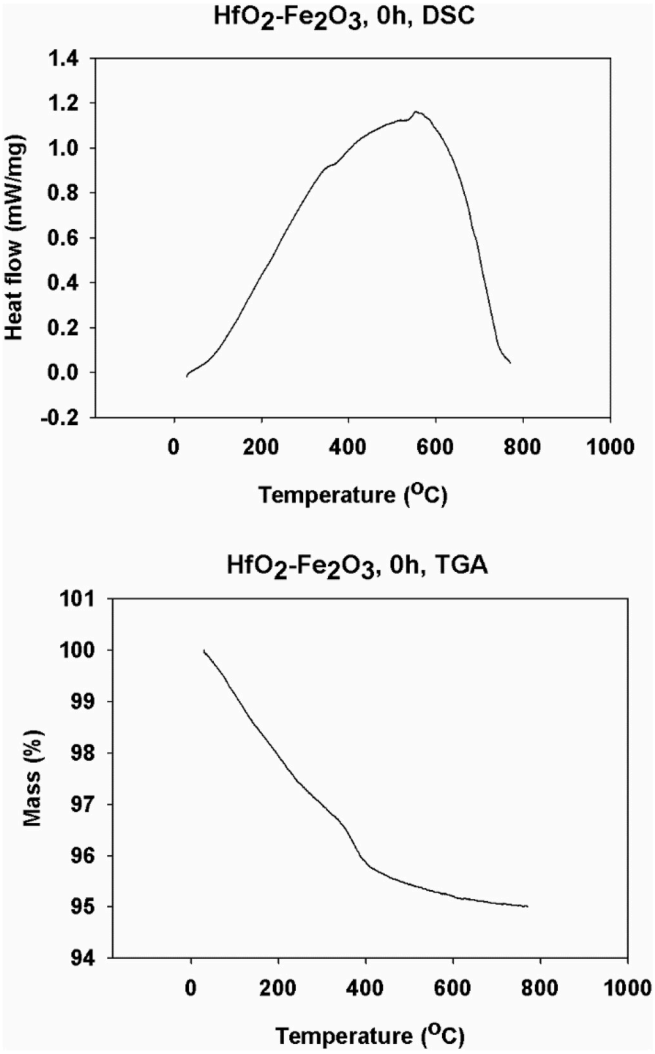

Fig. 17. DSC and TGA for equimolar hafnia-hematite unmilled.

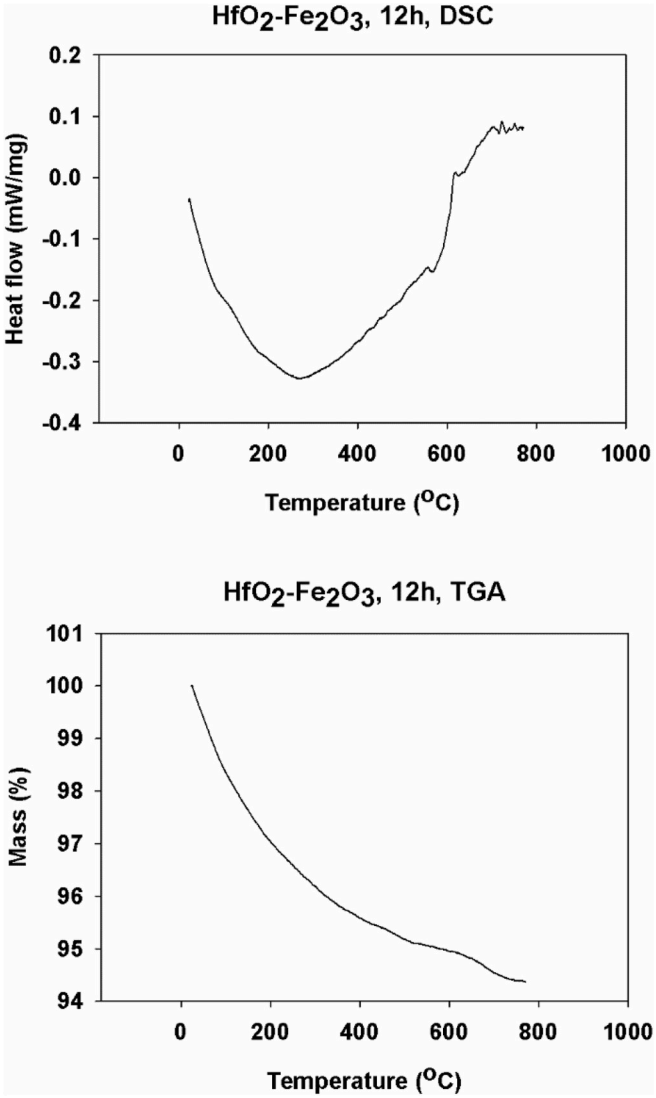

Fig. 18. DSC and TGA for equimolar hafnia-hematite after milling for 12 h.

Declaration of competing interest

The authors declare no conflicts of interest regarding the publication of this paper.

CRediT authorship contribution statement

Louise Ferris: Formal analysis. **Mark Allwes:** Formal analysis. **Lucian Diamandescu:** Formal analysis. **Alice Perrin:** Formal analysis. **Michael McHenry:** Formal analysis. **Monica Sorescu:** Formal analysis.

Acknowledgments

This work was supported by the National Science Foundation, USA under grants DMR-0854794 and DMR-1002627-1.

References

[1] L.F. Li, P. Tong, Y.M. Zou, W. Tong, W.B. Jiang, Y. Jiang, X.K. Zhang, J.C. Lin, M. Wang, C. Yang, X.B. Zhu, W.H. Song, Y.P. Sun, Good comprehensive performance of Laves phases $Hf_{1-x}Ta_xFe_2$ as negative thermal expansion materials, Acta Mater. 161 (2018) 258–265, https://doi.org/10.1016/j.actamat.2018.09.029.

[2] R. Govindaraj, C.S. Sundar, L. Seetha Lakshmi, V. Sridharan, M. Premila, D. V. Natarajan, Perturbed angular correlation studies in hafnium doped $La_{0.67}Ca_{0.33}MnO_3$, Chem. Phys. 302 (2004) 185–192, https://doi.org/10.1016/j.chemphys.2004.04.003.

[3] F. Delogu, L. Takacs, Information on the mechanism of mechanochemical reaction from detailed studies of the reaction kinetics, J. Mater. Sci. 53 (2018) 13331–13342, https://doi.org/10.1007/s10853-018-2090-1.

[4] C.Y. Chain, S. Ferrari, L.C. Damonte, J.A. Martinez, A.F. Pasquevich, Evolution of the quadrupole hyperfine interaction while milling a Si-HfO_2 blend, J. Alloys Compd. 5365 (2012) 550–554, https://doi.org/10.1016/j.jallcom.2012.02.082.

[5] M. Karabulut, A. Popa, C. Berghian-Grosan, H. Ertap, M. Tuksek, S. Tokdemir Ozturk, R. Stefan, On the structural features of iron-phosphate glasses by Raman and EPR: observation of superparamagnetic behavior differences in HfO_2 and CeO_2 containing glasses, J. Mol. Struct. 1191 (2019) 59–65, https://doi.org/10.1016/j.mol.struc.2019.04.086.

[6] T. Tsoncheva, R. Ivanova, J. Henych, N. Velinov, M. Kormunda, M. Dimitrov, D. Paneva, M. Slusna, I. Mitov, V. Stengl, Iron modified titanium-hafnium binary oxides as catalysts in total oxidation of ethyl acetate, Catal. Commun. 81 (2016) 14–19, https://doi.org/10.1016/j.catcom.2016.03.014.

[7] K. Wittle, G. Lumpkin, F. Berry, G. Oates, K. Smith, S. Yudintsev, N. Zaluzec, The structure and ordering of zirconium and hafnium containing garnets studies by electron channeling, neutron diffraction and Mössbauer spectroscopy, J. Solid State Chem. 180 (2007) 785–791, https://doi.org/10.1016/j.jssc.2006.12.006.

[8] Y. Sun, M. Koshimizu, N. Yahaba, F. Nishikido, S. Kishimoto, R. Haruki, K. Asai, High-energy X-ray detection by hafnium-doped organic-inorganic hybrid scintillators prepared by sol-gel method, Appl. Phys. Lett. 104 (2014) 174104, https://doi.org/10.1063/1.4875025.

[9] M. Karabulut, C. Aydin, H. Ertap, M. Yuksek, Structure and properties of hafnium iron borophosphate glass-ceramics, J. Non-Cryst. Solids 411 (2015) 19–25, https://doi.org/10.1016/j.jnoncrysol.2014.12.014.

[10] M. Karabulut, M. Yuksek, G.K. Marasinghe, D.E. Day, Structural features of hafnium iron phosphate glasses, J. Non-Cryst. Solids 355 (2009) 1571–1573, https://doi.org/10.1016/j.jnoncrysol.2009.06.005.

[11] M. Karabulut, H. Ertap, M. Yuksek, IR and Mössbauer spectroscopic study of cerium iron borophosphate glasses, J. Non-Cryst. Solids 417–418 (2015) 39–44, https://doi.org/10.1016/j.jnoncrysol.2015.03.012.

[12] A. Paesano, E.Y. Honda, M.A. Rocha, J.B.M. da Cunha, B. Hallouche, Solid state amorphization and crystallization in $Fe_{1-x}Hf_x$ multilayered films, Thin Solid Films 459 (2004) 165–172, https://doi.org/10.1016/j.tsf2003.12.132.

[13] G. Stefanic, B. Grzeta, K. Nomura, R. Trojko, S. Music, The influence of thermal treatment on phase development in ZrO_2-Fe_2O_3 and HfO_2-Fe_2O_3 systems, J. Alloys Compd. 327 (2001) 151–160.

[14] Monica Sorescu, Recent Applications of the Mössbauer Effect, Dorrance Publishing Company, Pittsburgh, 2020, ISBN 9781646104970.